

HiSST: 4th International Conference on High-Speed Vehicle Science Technology 22 -26 September 2025, Tours, France



Thermal non-equilibrium effects in the inviscid flow within high Mach number inlets

Dengke Li¹, Bo Sun^{1, a)}, and Xiong Chen¹

Abstract

The thermal non-equilibrium caused by the high temperature has significant impacts on the inviscid flows through the hypersonic inlets. However, there is limited research available that provides a comprehensive understanding of the impacts of thermal non-equilibrium on the flows of the inlets with wide design constraints. To explore the thermal non-equilibrium effects within the high Mach number inlets, the inviscid flows obtained by method of non-equilibrium characteristics are compared with the flow calculated under th¹e calorically perfect gas (CPG) assumption. The results reveal that the impacts of thermal non-equilibrium on the outlet Mach number and static temperature intensify with the increasing flight Mach number, compression level and capture height. The relative discrepancies in outlet Mach number and static temperature that induced by thermal non-equilibrium can exceed 10%. Those discrepancies stem from the redistribution of internal energy modes in the thermal nonequilibrium flow. It is found that the discrepancy in outlet static temperature shows a quasi-equal relationship with e_v/e_v at the outlet section, while the discrepancy in outlet Mach number exhibits a power-law correlation with e_v/e at the outlet section. Due to the scale effects of thermal nonequilibrium, the discrepancy in outlet Mach number rises from 4% to 10.4% as the capture height increases from 0.125 m to 2 m. The above insights provide valuable reference for the thermal nonequilibrium effects in the inviscid design and evaluation of high Mach number inlet for scramjets and oblique detonation engines.

Keywords: thermal non-equilibrium, inviscid flow, high Mach number inlet, scale effects, scramjets

1. Introduction

Scramjet and oblique detonation engines (ODEs) are the two typical air-breathing propulsion system for hypersonic vehicles. Those propulsion systems both consist of inlet, combustion chamber and nozzle. As the upstream component of the propulsion system, the performance of the inlet has evident impact on the thrust and specific impulse of the engine [1,2]. Therefore, it's of great importance to take sufficient effort on the design method and flow characteristic of inlets.

For the inlets operating at conventional hypersonic speed, the design method and flow features have been deeply explored. Recently, more and more research focus on the high Mach number ($Ma \ge 8$) inlets [3–5]. As the flight Mach number gradually increase, the total enthalpy of the freestream goes up. For inlet operating at high Mach number, the temperature after the strong shock wave and within the boundary layer can result in the vibrational energy excitation and chemical reactions. Due to the high flow speed, those processes have characteristic times that fall in same scales of the flow characteristic times. As a result, the physical properties of the gas vary as the flow developed downstream, thereby influencing the flow structure and inlet performance. Those phenomena are called the thermochemical non-equilibrium effects [6].

The previous studies indicated that the thermochemical non-equilibrium effects have significant impacts on the shock reflection [7], shock/shock interaction [8,9], and shock wave/boundary interaction [10,11], which are typical flow phenomena in the inlet. Therefore, several works were conducted to understand the thermochemical non-equilibrium effects in high Mach number inlet. Gehre et al. [12] numerically investigated the thermal non-equilibrium effects in an inlet with freestream total enthalpy from 3.3 to 4.9 MJ/kg. The numerical results indicated that the thermal non-equilibrium gas (TNG) model exhibits higher static temperature within the boundary layer than the thermal perfect gas (TPG) model. Dai et

HiSST-2025-0056 Page | 1 Thermal non-equilibrium effects in the inviscid flow within high Mach number inlets Copyright © 2025 by author(s)

1

¹ School of Mechanical Engineering, Key Laboratory of Special Engine Technology, Ministry of Education, Nanjing University of Science and Technology, Nanjing, 210094, China, hypersun@126.com

al. [13–15] conducted several studies on the thermochemical non-equilibrium effects in high Mach number inlet. For a curve compression inlet with a design Mach number of 12, they found that the outlet static temperature calculated under the assumption of the calorically perfect gas (CPG) was 10.52%

higher than that of a thermochemical non-equilibrium gas (TCNEG) model. Conversely, the thermochemical non-equilibrium effects resulted in an increase of 7.69% in the exit total pressure recovery compared to the results of CPG model. In addition, they have pointed out that the thermal non-equilibrium has greater impacts on the inlet performance. This is because the thermal nonequilibrium occurs in almost the whole flow field of the inlet, while the air dissociation mainly takes place in the boundary layer of the internal flow path. For an inward-turning inlet operating at Mach 12, it is found that the development of stream-wise vortex could be impacted by the thermochemical nonequilibrium effects. Wu et al. [16] investigated the effects of thermal non-equilibrium on the flow capture capacity of inlet. It has been found that the thermal non-equilibrium effects thermal nonequilibrium effects could lead to a reduction of 10.7% compared to the results calculated by thermal perfect gas (TPG) model at Mach 8. Zuo et al. [17] investigated the effects of wall temperature on the thermochemical non-equilibrium flow of a wavecatcher inlet at Mach 12. The results have shown that the dissociation degree of the oxygen gradually increases as the wall temperature goes up. For an adiabatic wall, the maximum degree of oxygen dissociation reaches 54.0% at the symmetry plane. In summary, the thermal non-equilibrium effects play an important role in the mainstream and boundary layer of the inlet. The chemical non-equilibrium effects mainly affect the inlet performance by changing the gas properties in the boundary layer. Therefore, the thermal non-equilibrium effect is the key phenomenon that should be considered in the inviscid design of inlet.

Though the previous studies provided a deep understanding of the thermal non-equilibrium effects on the high Mach number inlets, the most of the studies are limited to a given inlet design point and the inlet lengths are less than 2.5 m. In the engineering design of inlets, the flight Mach number, compression level and geometry constraints should be changed to meet different overall design requirements of the vehicle. With different design requirements, the impacts of thermal non-equilibrium on the inlet vary. The conclusions obtained from a limited number of inlet configurations are too special to provide a quantity understanding of the thermal non-equilibrium effects for inlets with different design requirements. The influence level of thermal non-equilibrium on the inviscid design of inlet under wide design space remains unknown. To address this gap, this paper aims to clarify the impacts of thermal non-equilibrium on the inlet flow and performance. First, the case configuration and numerical method are introduced. Then, the thermal non-equilibrium effects on the inlets with different design constraints are obtained by comparing the results based on CPG and TNG model. Finally, the main conclusions are given.

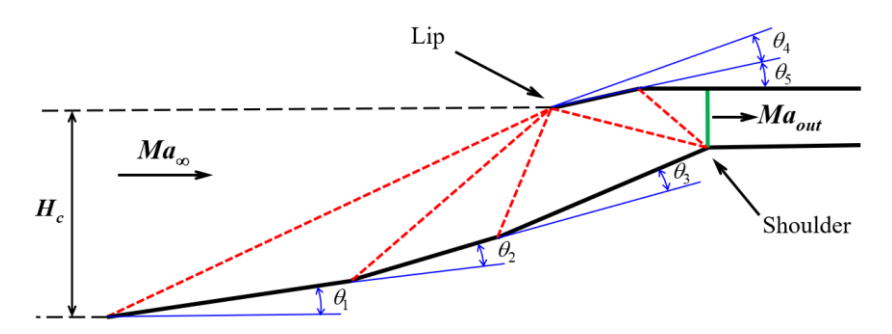


Fig 1. Schematic of inlet geometry.

Table 1Flow parameters for flight Mach number ranging from 8 to 15.

$\overline{\mathit{Ma}_{\infty}}$	H_{∞} /km	p∞/Pa	$T_{t,\infty}$ /K	h ₀ /(MJ/kg)	
8	30.47	1115.92	226.97	3.15	
10	33.49	714.33	232.33	4.92	
12	36.03	496.4	239.37	7.19	

15 39.26 317.38 248.30 11.51	15	39.26	317.38	248.30	11.51	
------------------------------	----	-------	--------	--------	-------	--

2. Physical models and numerical method

2.1. Case configuration

The planar compression inlet consists of the external compression with three shock waves and the internal compression with two shock waves. As shown in Fig.1, the inlet profile and shock waves are represented by the solid line in black and dashed line in red, respectively. The three shock waves for external compression need to converge at lip to improve the compression efficiency and ensure the full capture of incoming stream. The two internal compression shock waves should be converged on the shoulder to suppress the reflection of shock waves downstream of the throat by using the shoulder expansion waves. The throat section is selected as the outlet section to evaluate the inlet performance. Considering the engineering requirement, the stream should turn to horizontal direction at the throat. So, the deflection angles of each wedge must meet:

$$\theta_1 + \theta_2 + \theta_3 = \theta_4 + \theta_5 \tag{1}$$

The flight conditions from Mach 8 to 15 are involved in the present study. It is assumed that the air is made of nitrogen and oxygen, with mass fractions of 0.77 and 0.23, respectively. The free stream is assumed to be in a thermal equilibrium state. All flight altitudes correspond to a dynamic pressure of 50 kPa, which falls within the flight envelope appropriate for high Mach number scramjet. The detailed incoming parameters are presented in Table 1.

Table 2 Values of the design constraints

 $Ma_{r,design}$	H_c /m
0.3, 0.325, 0.35, 0.375, 0.4, 0.45, 0.5	0.125, 0.25, 0.5, 1, 1.5, 2

The values of the design constraints are shown in Table 2, including 168 cases. Currently, there is no definitive principle regarding the compression level of inlet for the supersonic combustion. In the design of conventional hypersonic inlet, the outlet Mach number is often set at approximately half of the flight Mach number [18,19]. Whereas, this design constraint is not conducive to the effective organization of downstream combustion for engines operating at high Mach number. For instance, the outlet Mach number of the inlet will achieve 6 when the flight Mach number is 12, which is almost impossible for the efficient mixing and combustion. Additionally, the extremely high compression level may cause strong dissociation in the boundary layer, thereby reducing the heat release of combustion. Taking these factors into account, the upper limit of the ratio of outlet Mach number to the flight Mach number ($Ma_{r,design}$) is set as 0.5, the lower limit is set as 0.3.

Since non-equilibrium effects are jointly determined by the thermochemical processes and flow evolution, the impact degree of the thermal non-equilibrium is very sensitive to the inlet length. When Ma_{∞} and $Ma_{r,design}$ are given, the capture height H_c determines the length of the inlet. Therefore, the scale effects of thermal non-equilibrium are assessed by varying H_c . In present study, H_c ranges from 0.125 to 2 m, encompassing most of the length scales of inlets in the wind tunnel tests and real vehicles.

As described above, the design constraints for a given flight Mach number are H_c , $Ma_{r,design}$ and Eq. (1). The optimization goal is maximizing the total pressure recovery. The gas dynamic functions [6,20] under CPG assumption and sequential least squares quadratic programming (SLSOP) [21] are employed

under CPG assumption and sequential least squares quadratic programming (SLSQP) [21] are employed to solve this multi-constrained nonlinear optimization problem. The similar design procedures have been applied in a number of studies [18,19,22,23], which are not described in details here. The optimal configuration of the three external compression shock and the two internal compression shocks both satisfy the principle of equal strength [24], which shows good agreement with the design results proposed by Smart [22].

2.2. Gas models and numerical method

The calorically perfect gas (CPG) and thermal non-equilibrium gas (TNG) model are used for simulating the inviscid flow of the inlets to obtain the impacts of thermal non-equilibrium on the inlets. Under the CPG assumption, the energy transfer between the different internal energy modes is neglected. Only the translational-rotational energy mode is taken into account and the specific heat ratio is treated as a constant value of 1.4. Under the CPG model, the inviscid flow can be solved by the basic gas dynamic relations [20,25] across the shock waves.

As for the flow condition in this study, the possible thermal non-equilibrium processes primarily contain rotational-translational (R-T) energy transfer, vibrational-translational (V-T) energy transfer, and vibrational-vibrational (V-V) energy transfer. Given that the timescales of R-T energy transfer are only a few nanoseconds, the translational energy mode and rotational energy mode are assumed to be in equilibrium and can be characterized by a translational-rotational temperature T_i (static temperature). The Park's two-temperature model [26] is selected to model the V-T energy transfer. The V-V energy transfer is neglected and the vibrational energy mode of each molecular species is characterized by a single vibrational temperature T_{ν} . Consequently, the V-T energy transfer is the main difference between the TNG and CPG model. Besides the basic Euler equations, an extra equation for vibrational energy is involved in the governing equations for TNG model:

$$\rho \frac{De_{v}}{Dt} = \omega_{v} \tag{2}$$

where ρ and e_v are the density and specific vibrational energy, respectively. The vibrational energy source term ω_v is calculated following the Landau-Teller model [27]:

$$\omega_{v} = \sum_{s=1}^{n} \rho_{s} \frac{e_{v,s}(T_{t}) - e_{v,s}(T_{v})}{\tau_{s}}$$
(3)

where τ_s represents the vibrational relaxation time, which can be calculated by the semi empirical formula summarized by Millikan and White [28].

For diatomic molecules, the specific internal energy can be calculated using the following formula:

$$e_s = e_{tr,s} + e_{v,s} \tag{4}$$

where the specie's translational-rotational energy and vibrational energy per unit mass can be expressed as:

$$e_{tr,s} = \frac{5}{2} R_s T_t \tag{5}$$

$$e_{v,s} = \frac{\mathcal{G}_{v,s} R_s}{\exp(\mathcal{G}_{v,s} / T_v) - 1}$$
(6)

where R_s is the gas constant for species s. The vibrational characteristic time is represented by $\mathcal{G}_{v,s}$, with values of 3371 K and 2256 K for nitrogen and oxygen, respectively. The specific heat at constant volume involves the parts of translational-rotational energy mode and vibrational energy mode that can be calculated as:

$$c_{v(tr,s)} = \frac{5}{2}R_s \tag{7}$$

$$c_{v(v,s)} = \frac{de_{v,s}}{dT_v} = \frac{g_{v,s}^2 R_s \exp(g_{v,s} / T_v)}{T_v^2 (\exp(g_{v,s} / T_v) - 1)^2}$$
(8)

The specific heat at constant pressure for species s can be calculated by:

$$c_{p,s} = c_{v,s} + R_s \tag{9}$$

For the gas mixture, the total thermodynamic properties are the weighted average of mass fraction for each species:

$$\phi = \sum_{s=1}^{n} Y_s \phi_s \tag{10}$$

where Y_s represents the mass fraction of specie s, ϕ involves the energy modes, specific heat at constant volume and specific heat at constant pressure.

The method of non-equilibrium characteristic (MONC) [29] is used to solve the inviscid flow with thermal non-equilibrium process for its high fidelity and efficiency. In the previous study, MONC was rigorously validated against non-equilibrium flow scenarios encompassing curved compression surfaces, blunted wedges and internal nozzle flows. The validation results indicated that MONC is capable of predicting numerical results with a deviation of less than 2% from computational fluid dynamics (CFD) results obtained by hy2Foam [30,31].

3. Results and discussion

3.1. Thermal non-equilibrium flow characteristics under a typical condition

To recognize the fundamental characteristics of the inlet flow, the inlet flow with $Ma_{\infty}=12$, $H_c=1\,\mathrm{m}$, and $Ma_{r,design}=0.4$ is analyzed first. Fig 2. illustrates the temperature distribution of the inlet flow. The shock waves and streamline are represented by the solid lines in red and black, respectively. The parameters along the streamline are shown in Fig. 3. The symbol SW_i is used to represent the shock wave. Since the static temperature is just around 520 K, the collision frequency of the molecules is not enough to make an evident change on the vibrational energy mode in such a short flow time, the vibrational temperature remains the same with the freestream in the upstream region the third shock wave. The Mach number and static temperature calculated by CPG and TNG model are highly consistent here. Downstream of the third shock wave, the static temperature reaches 780 K , the vibrational temperature increases along the streamwise, achieving 412 K. While the Mach number and static temperature keep unchanged. The difference between the results on the streamline obtained by CPG and TNG model is below 0.5%.

In the downstream region of the first internal compression shock wave, a considerable part of the internal energy is gradually transferred from the translational-rotational mode to the vibrational mode, so the vibrational temperature and Mach number gradually increase along the flow direction, and the translational-rotational temperature gradually decreases along the flow direction. Upstream of the second internal compression shock, the static temperature along the streamline computed by TNG model shows a 0.7% reduction compared to the CPG assessment, while the Mach number increases by approximately 1%. Downstream of the final shock, thermochemical nonequilibrium effects intensify substantially. At the outlet position, the TNG computation shows approximately 4.4% reduction in static temperature and 4.9% increase in Mach number compared to evaluation based on CPG model.

The increasing trend of Mach number downstream of the two internal compression shocks stems from the reduced static temperature and specific heat ratio due to V-T energy exchange, which in turn decreases the local speed of sound. Comparing the static temperature and vibrational temperature, it can be found that the reduction in static temperature is significantly less than the increase in vibrational temperature. This discrepancy arises from the fact that the translational-rotational energy mode of a diatomic molecule has five thermal degrees of freedom, whereas the vibrational mode contains only two thermal degrees of freedom. Therefore, vibrational temperature is more sensitive to the energy exchange between the energy modes.

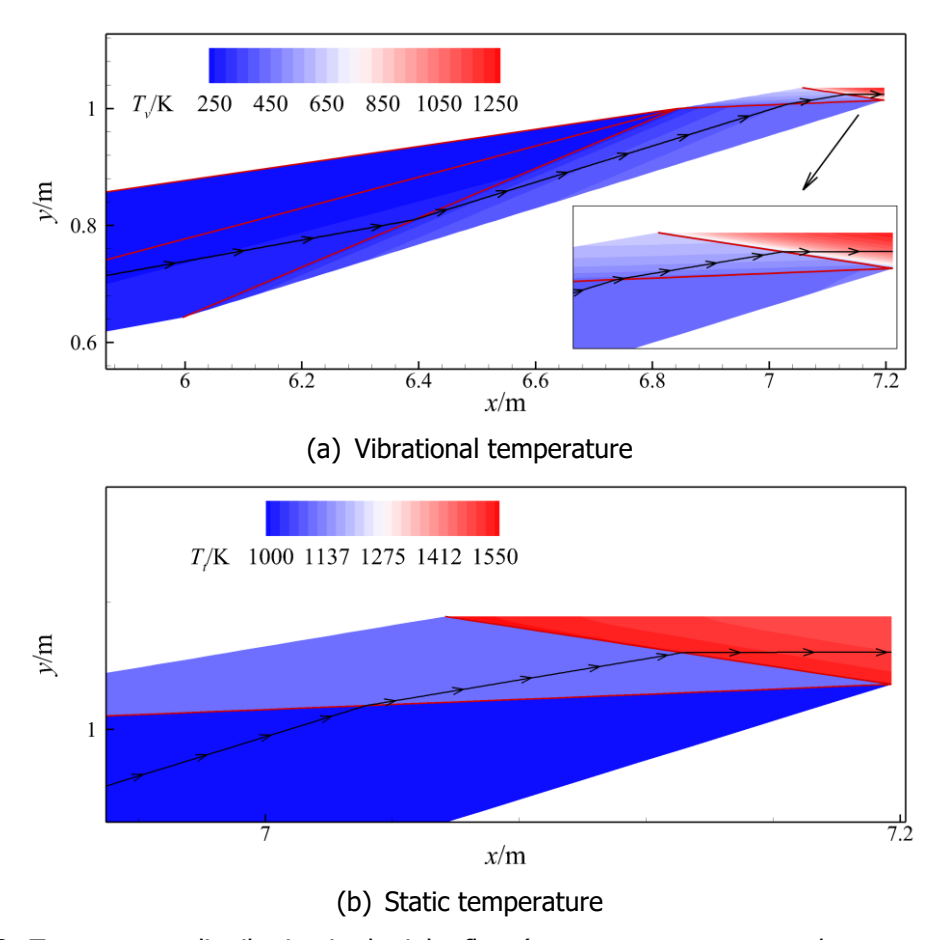


Fig 2. Temperature distribution in the inlet flow ($Ma_{\infty} = 12$, $H_c = 1$ m, and $Ma_{r,design} = 0.4$)

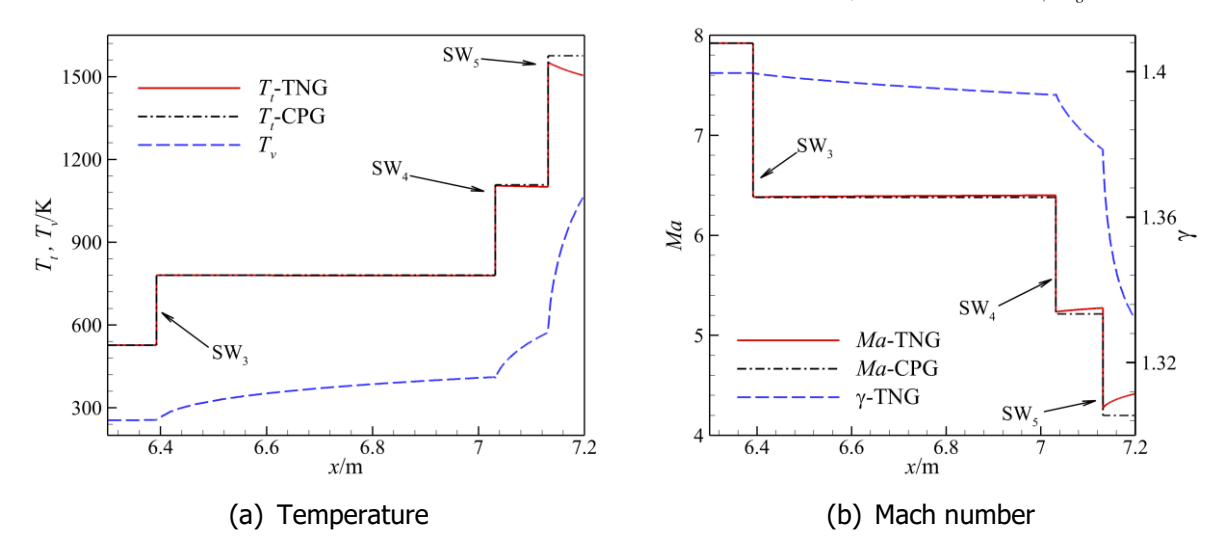


Fig 3. Temperature and Mach number along the streamline

The thermal non-equilibrium process can also lead to a non-uniform distribution of parameters along the normal direction. The parameter distribution on the outlet section is given in Fig. 4 to obtain the non-uniform distribution law. As the height increases, the Mach number exhibits a gradual rise from 4.28 to 4.46, while the static temperature gradually decreases from 1544 K to 1482 K, and the vibrational temperature increases from 559 K to 1234 K. Notably, in the vicinity of the upper wall, the discrepancies between the results of the two gas models are the highest, meaning that the impacts of thermal non-equilibrium are the strongest. The relative discrepancies reach 6.2% in Mach number and 5.9% in static temperature. The non-uniform distribution of parameters is predominantly governed by molecular collision frequency and post-shock flow distance. The larger the static temperature and

density, the higher the molecular collision frequency. Additionally, a longer post-shock distance enables more flow time for V-T energy transfer. At the region near the upper wall, the flow distance after the two internal shock is the longest, and the static temperature is high. Therefore, the V-T energy transfer is the most sufficient at the region near the upper wall, resulting in the largest discrepancy between the results obtained from the two gas models.

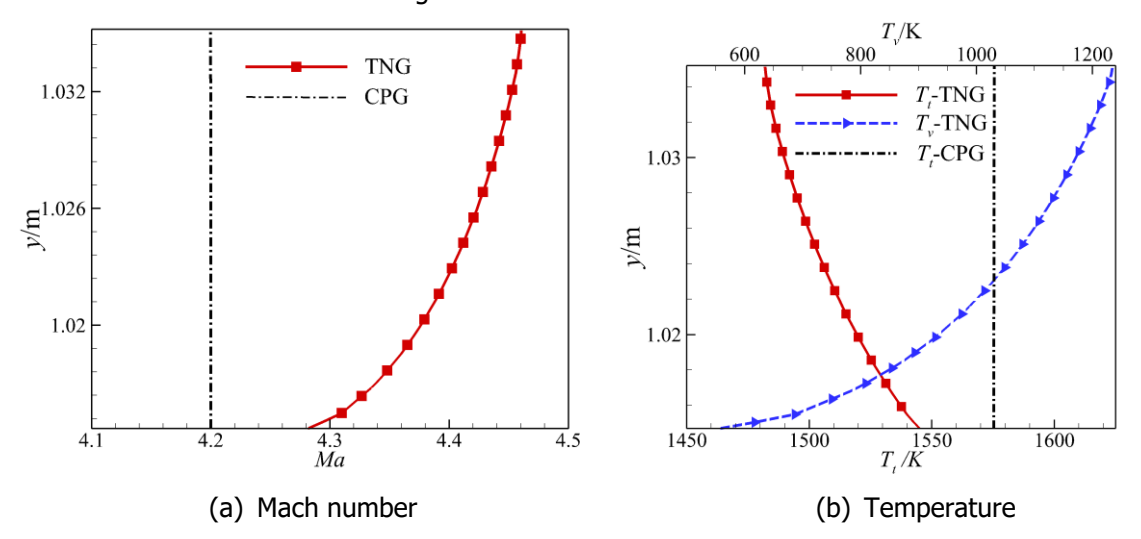


Fig 4. Parameters distribution on the outlet section on inlet.

To sum up, V-T energy transfer results in a higher Mach number and a lower static temperature compared to the CPG-based evaluation. The impacts of thermal non-equilibrium accumulate rapidly along the flow direction in the downstream region of the two internal compression shocks, with the most significant impact observed on the upper wall side of the outlet section.

3.2. Effects of thermal non-equilibrium on outlet parameters

The mass-weighted average of parameters at the outlet section can be calculated as:

$$\phi_{out} = \frac{\int_{A} \rho \phi dA}{\int_{A} \phi dA} \tag{11}$$

where ϕ is the parameter at the outlet section; dA is the area element of the outlet section. For the present two-dimensional flow, the differential length element is used in the integration. The relative discrepancies in the mass-weighted average of parameters at the outlet section evaluated by the CPG and TNG model is used to reflect the impacts of thermal non-equilibrium, which can be expressed as:

$$\Delta \phi_{out} = \frac{\left|\phi_{out,CPG} - \phi_{out,TNG}\right|}{\phi_{out,CPG}} \times 100\%$$
(12)

It's clear that a higher $\Delta\phi_{out}$ means a stronger impact of thermal non-equilibrium on the inlet performance.

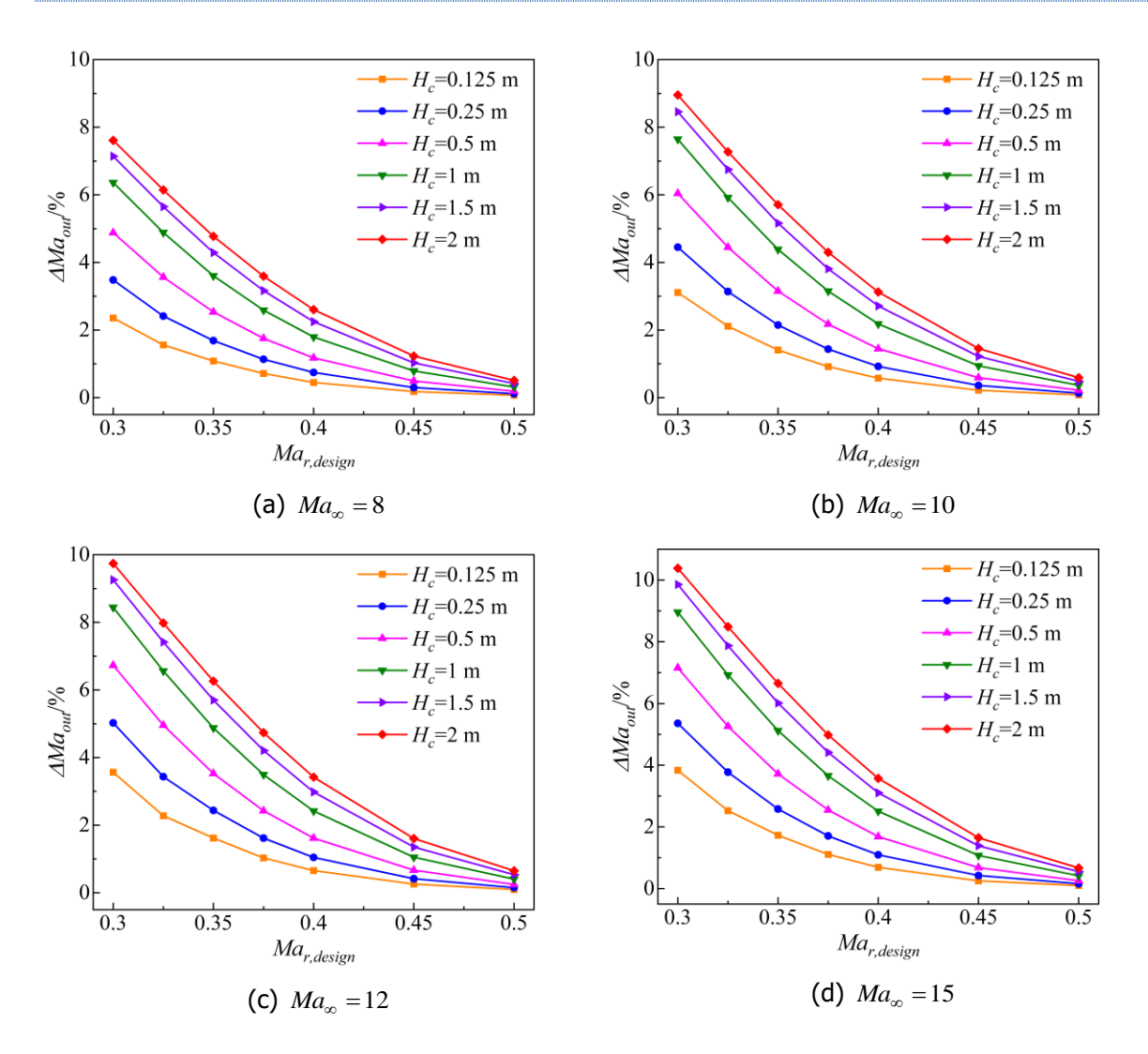
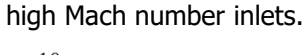


Fig 5. The relative discrepancies in outlet Mach number under different sets of design constraints

Fig. 5 depicts the ΔMa_{out} under different sets of design constraints. When $Ma_{r,design}=0.5$, the ΔMa_{out} under all the design constraints are lower than 1%. This indicates that the CPG model can still be employed in the inviscid design process when $Ma_{r,design}\geq 0.5$. As $Ma_{r,design}$ declines, the ΔMa_{out} gradually goes up with an increasing rate. Selecting the curve with $Ma_{\infty}=12$ and $H_c=1$ m for instance, the ΔMa_{out} increases from 0.4% to 8.4% as $Ma_{r,design}$ declines from 0.5 to 0.3. Comparing the ΔMa_{out} at different flight Mach number , one can find that the higher the flight Mach number, the larger the ΔMa_{out} . Under design constraints of $H_c=1$ m and $Ma_{r,design}=0.3$, an increase in flight Mach number from 8 to 15 causes ΔMa_{out} to rise from 7.6% to 10.4%. This increases in ΔMa_{out} caused by changes in $Ma_{r,design}$ and Ma_{∞} can both be attributed to the rise of static temperature in the inlet flow. A higher static temperature means a higher the collision frequency of molecules, which is conductive to the V-T energy transfer.

By comparing the curves with different H_c , one can conclude that the increase in H_c results in larger ΔMa_{out} when the other design constraints are the same. When $Ma_{\infty}=12$ and $Ma_{r,design}=0.3$, ΔMa_{out} grows from 3.6% to 9.7% with increasing H_c . This is because that a larger H_c means a longer inlet length, thereby increasing the flow time for V-T energy transfer. The more energy transforms from translational-rotational energy mode to vibrational mode, the larger the ΔMa_{out} . This phenomenon manifests the scale effects of thermal nonequilibrium on flow dynamics. Consequently, the influence of thermal nonequilibrium scale effects must be prioritized in designing and evaluating inviscid flows within



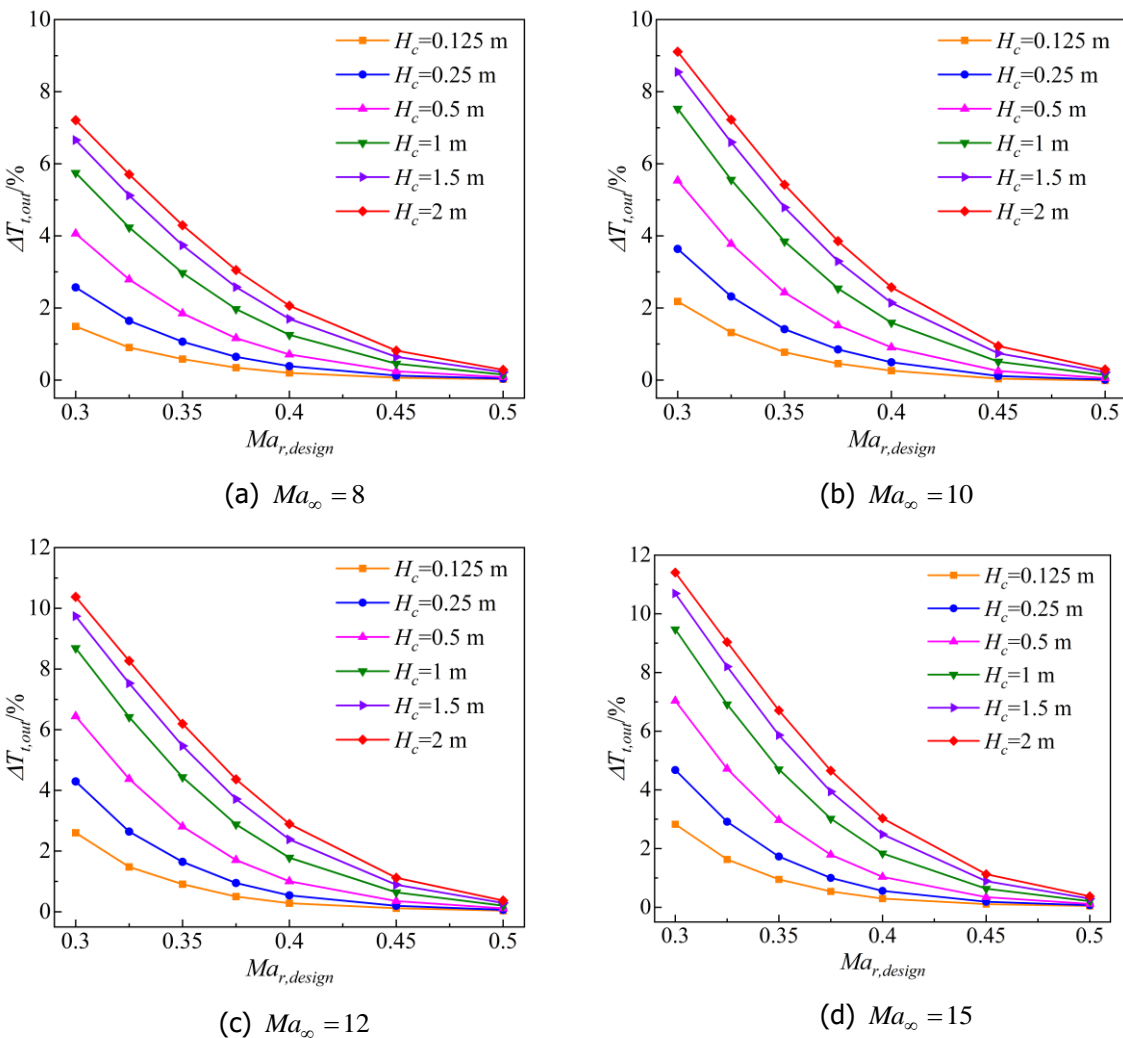


Fig 6. The relative discrepancies in static temperature at outlet section under different design constraints

As shown in Fig. 6, the influence regularities of design constraints on $\Delta T_{t,out}$ are similar to those of ΔMa_{out} . Increasing the compression level, the flight Mach number or the capture height all lead to larger $\Delta T_{t,out}$. When $H_c=2$ m, $Ma_{\infty}=15$ and $Ma_{r,design}=0.3$, the $\Delta T_{t,out}$ reaches its maximum of 11.4%. In the design and assessment of engines, using the CPG model may overpredict the static temperature at the inlet outlet, potentially leading to errors in calculating fuel ignition and heat release characteristics.

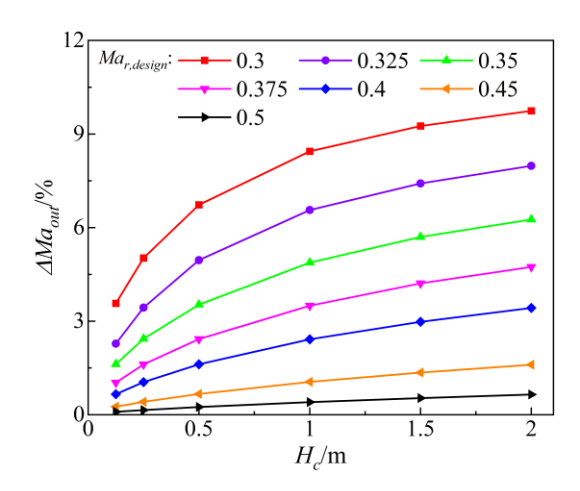
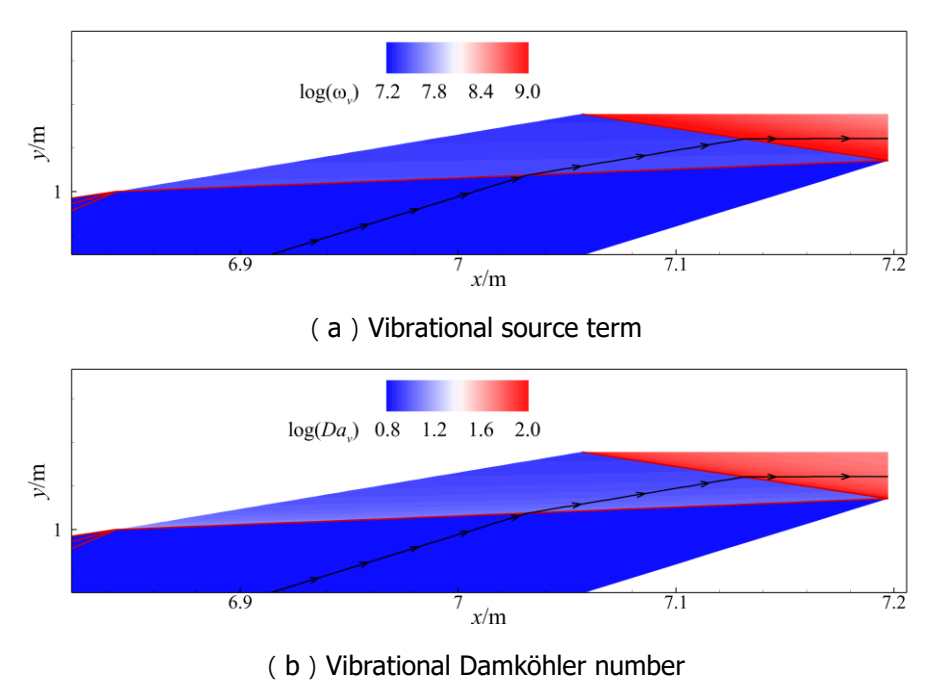
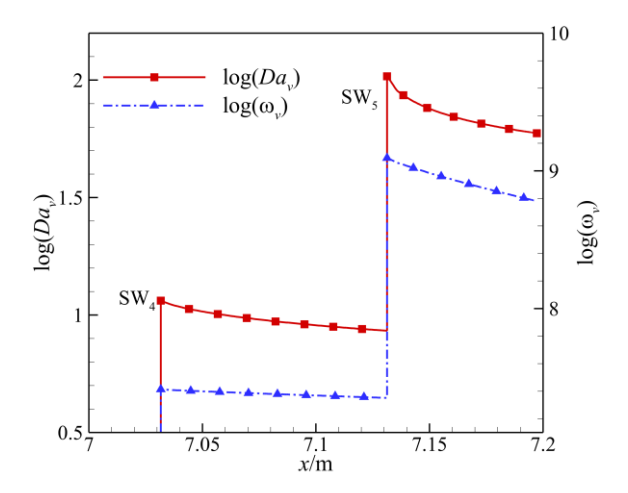


Fig 7. ΔMa_{out} versus H_c with different compression level ($Ma_{\infty} = 12$)

The variation curve of ΔMa_{out} with H_c at flight Mach number of 12 is illustrated in Fig. 7 to further investigate the thermal non-equilibrium scale effects in the inlet flow. As H_c goes up, the slope of each curve gradually decreases, indicating that the influence of thermal non-equilibrium scale effects on the flow weakens with an enhancing \boldsymbol{H}_{c} . To understand the underlining physics of such regularity, the distribution of vibrational Damköhler number Da_{ν} and ω_{ν} are analyzed in the following text. The detailed calculation of Da_v can be found in Refs. [8,32]. Fig. 8 depicts the distribution of Da_v and ω_v under the design constraints of $Ma_{\infty}=12$, $Ma_{r,design}=0.35$, and $H_c=1$ m. In the downstream region of the two internal compression shocks, ω_{ij} decreases along the flow direction, meaning that the excitation rate of vibrational energy gradually goes down as flow develops. The decrease of ω_{ij} is mainly caused by two factors. The first factor is that the difference between local vibrational energy and the corresponding equilibrium vibrational energy decreases as flow develops downstream, meaning that the gas is approaching thermal equilibrium state. The second factor is that the reduction of static temperature along the flow direction leads to longer vibrational relaxation time for molecules. This extend of the vibrational characteristic time reduces Da_v as well, indicating that the flow is develops towards a thermal frozen state. Overall, the increase in H_c reduces the average excitation rate for vibrational energy, which is the main reason for the weakening impact of thermal non-equilibrium scale effects.





(c) Vibrational source term and vibrational Damköhler number along the streamline

Fig 8. Distribution of vibrational source term and vibrational Damköhler number in the inlet flow $(Ma_{\infty} = 12, Ma_{r,design} = 0.35, H_c = 1 \text{ m})$

To better explain the relationship between the V-T energy transfer and the discrepancies in outlet Mach number and static temperature, the state of internal energy distribution is characterized by the vibrational energy fraction e_v / e . The data of $\Delta T_{t,out}$ and ΔMa_{out} versus e_v / e is shown in Fig. 9. It can be found that there is a linear relationship between $\Delta T_{t,out}$ and e_v / e . The expression can be obtained by linear regression:

$$\Delta T_{t,out} = 0.9915 \left(\frac{e_{\nu}}{e}\right) + 0.01665 \tag{13}$$

The coefficient of determination (R^2) corresponding to the linear fitting formula is 0.9997. The slope of the formula is very close to 1 and the intercept is close to 0, meaning that $\Delta T_{t,out}$ is almost equal to the e_v /e at the outlet section. The underlining physics can be summarized into two aspects. On the one hand, the static temperature of diatomic molecules is proportional to the translational-rotational energy. On the other hand, the increase in vibrational energy is almost entirely originated by the V-T energy transfer. The increase in e_v /e is equal to the decrease of e_{tr} /e.

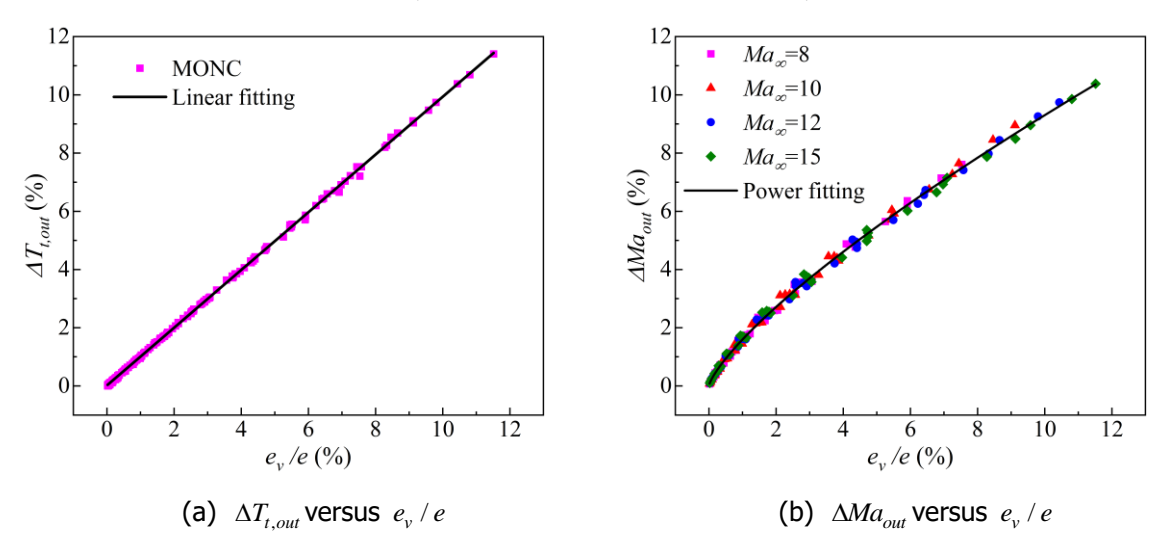


Fig 9. The discrepancies in outlet static temperature and Mach number varies with e_v / e

As shown in Fig. 19(b), the increasing rate of ΔMa_{out} declines as e_v / e increases. Remarkably, all data points collapse onto a single curve exhibiting a power-law trend. The fitted relationship between ΔMa_{out}

and e_v / e can be expressed as:

$$\Delta Ma_{out} = 1.593 \left(\frac{e_{v}}{e}\right)^{0.7663} \tag{14}$$

This equation also has a high R^2 of 0.997, indicating that a power-law correlation exists between ΔMa_{out} and e_v / e . Such power-law correlation can be explained by the equation of local speed of sound: $a = \sqrt{\gamma RT_t}$. First of all, ΔMa_{out} is mainly due to the relative discrepancy in the local speed of sound calculated by CPG and TNG model. There is a power-law relationship between a and γT_t . Secondly, $\Delta T_{t,out}$ and e_v / e exhibit a linear relationship. As shown in Fig. 10, e_v / e and $\Delta \gamma_{out}$ approximately satisfy a power-law correlation as well. Therefore, the relative discrepancy in the local speed of sound and e_v / e follow a power-law relationship. Based on the above relationships, one can inferred that ΔMa_{out} and e_v / e follow a power-law correlation. To sum up, the relationships among ΔMa_{out} , $\Delta T_{t,out}$, and e_v / e further clarifies that the ΔMa_{out} and $\Delta T_{t,out}$ is originated from the differences in the distribution of internal energy modes due to the V-T energy transfer.

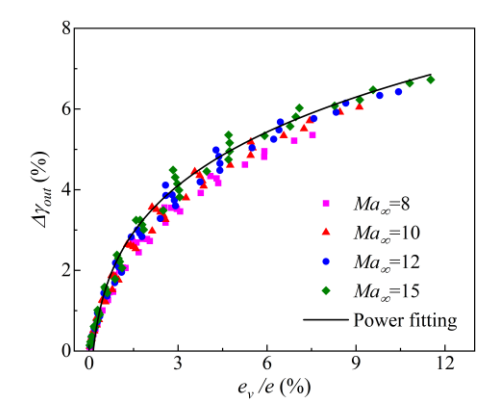


Fig 10. Variations of $\Delta \gamma_{out}$ with e_v/e .

4. Conclusions

To reveal the impacts of thermal non-equilibrium effects on the flow field and inlet performance, the inviscid flows of two-dimensional multi-stage compression inlets with the various design constraints are numerically predicted by using the CPG and TNG models. The key conclusions are summarized below:

- (1) The V-T energy transfer downstream of the shock waves results in the increase of Mach number, and the decline of static temperature along the flow direction. The thermal non-equilibrium effects have greater impacts in the flow near the upper wall than the flow near the lower wall, since the gas molecules undergo a long time under high temperature.
- (2) The difference on the distribution of the internal energy modes is the origin for the discrepancies in outlet Mach number and outlet static temperature calculated by the TNG and CPG model. The results suggests that $\Delta T_{t,out}$ shows a quasi-equal relationship with e_v / e at the outlet section, while ΔMa_{out} exhibits a power-law correlation with e_v / e at the outlet section.
- (3) The increases of capture height, compression level and flight Mach number intensify the impacts of thermal non-equilibrium on the outlet Mach number and static temperature. For inlet with $Ma_{\infty}=15$, $Ma_{r,design}=0.3$ and $H_c=2$ m, the thermal non-equilibrium can induce 10.4% increase in outlet Mach number and 11.4% decline in outlet static temperature.
- (4) The scale effects of thermal non-equilibrium have evident impacts on the outlet parameters. For inlets with $Ma_{\infty}=15$, $Ma_{r,design}=0.3$, the discrepancy in outlet Mach number rises from 4% to 10.4% as the capture height increases from 0.125 to 2 m. In addition, the impacts of scale effects of thermal non-equilibrium weaken with a increasing capture height.

Acknowledgments

This work was co-supported by the Aviation Science Foundation of China (20230012059001) and Training Fund for Excellent Doctoral Candidates of Nanjing University of Science and Technology.

References

- 1. M.K. Smart, How Much Compression Should a Scramjet Inlet Do?, AIAA Journal 50 (2012) 610–619.
- 2. W. Heiser, D. Pratt, D. Daley, U. Mehta, Hypersonic Airbreathing Propulsion, American Institute of Aeronautics and Astronautics, Inc., Washington, DC, 1994.
- 3. D.A. Ault, D.M. Van Wie, Experimental and computational results for the external flowfield of a scramjet inlet, J Propul Power 10 (1994) 533–539.
- 4. D.M. Van Wie, D.G. Drewry Jr., D.E. King, C.M. Hudson, The hypersonic environment: Required operating conditions and design challenges, J Mater Sci 39 (2004) 5915–5924.
- 5. J.E. Barth, D.J. Wise, V. Wheatley, M.K. Smart, Tailored Fuel Injection for Performance Enhancement in a Mach 12 Scramjet Engine, Journal of Propulsion and Power 35 (2019) 72–86.
- 6. J.D. Anderson, Hypersonic and High-Temperature Gas Dynamics, Third Edition, American Institute of Aeronautics and Astronautics, Inc., Reston, VA, 2019.
- 7. J. Peng, Z. Zhang, Z. Hu, Z. Jiang, A theoretical and computational study of the vibration excitation on the transition criteria of shock wave reflections, Aerosp Sci Technol 89 (2019) 299–306.
- 8. D. Li, B. Sun, C. Dai, X. Chen, Y. Man, Thermo-chemical non-equilibrium flows and aerodynamic loads of Type III shock/shock interaction on blunted lip of a Mach 12 inlet, Aerosp Sci Technol 161 (2025) 110168.
- 9. D. Li, B. Sun, C. Dai, X. Chen, X. Zhang, Y. Man, Influences of thermochemical non-equilibrium effects on Type III shock/shock interaction at Mach 10, Acta Astronaut 214 (2024) 553–566.
- 10. J. Hao, C.Y. Wen, J. Wang, Numerical investigation of hypervelocity shock-wave/boundary-layer interactions over a double-wedge configuration, International Journal of Heat and Mass Transfer 138 (2019) 277–292.
- 11. C. Dai, B. Sun, D. Zhao, S. Zhou, C. Zhou, Y. Man, High temperature non-equilibrium flow characteristics of impinging shock/flat-plate turbulent boundary layer interaction at Mach 8.42, Physics of Fluids 35 (2023) 095128.
- 12. R.M. Gehre, V. Wheatley, R.R. Boyce, Computational Investigation of Thermal Nonequilibrium Effects in Scramjet Geometries, J Propul Power 29 (2013) 648–660.
- 13. C. Dai, B. Sun, L. Yue, S. Zhou, C. Zhuo, C. Zhou, J. Yu, Thermochemical non-equilibrium flow characteristics of high Mach number inlet in a wide operation range, Chinese Journal of Aeronautics 36 (2023) 164–184.
- 14. C. Dai, B. Sun, S. Zhou, C. Zhuo, C. Zhou, L. Yue, Influence of high temperature non-equilibrium effects on Mach 12 scramjet inlet, Acta Astronaut 193 (2022) 237–254.
- 15. C. Dai, B. Sun, C. Zhou, C. Zhuo, L. Du, S. Zhou, Numerical investigation of real-gas effect of inward-turning inlet at Mach 12, Aerosp Sci Technol 115 (2021) 106786.
- 16. Y. Wu, J. Liu, J. Peng, X. Xu, B. Chen, Q. Yang, Effect of Thermal Nonequilibrium on Captured Mass Flow Rate of Scramjet Inlets, AIAA Journal (2023) 1–14.
- 17. F.-Y. Zuo, S. Mölder, S.-L. Hu, Thermochemical non-equilibrium effects on hypersonic wavecatcher inlet at Mach 12, Acta Astronaut 198 (2022) 56–68.
- 18. N.O.P. Raj, K. Venkatasubbaiah, A new approach for the design of hypersonic scramjet inlets,

- Phys Fluids 24 (2012) 086103.
- 19. Y. Li, L. Yue, C. He, W. Wu, H. Chen, Lagrange Optimization of Shock Waves for Two-Dimensional Hypersonic Inlet with Geometric Constraints, Aerospace-Basel 9 (2022) 625.
- 20. A. Achterberg, Gas Dynamics, Atlantis Press, Paris, 2016.
- 21. E. Bressert, SciPy and NumPy: An Overview for Developers, 1st edition, O'Reilly Media, Beijing Köln, 2012.
- 22. M.K. Smart, Optimization of Two-Dimensional Scramjet Inlets, J Aircraft 36 (1999) 430–433.
- 23. P.P.B. Araújo, M.V.S. Pereira, G.S. Marinho, J.F.A. Martos, P.G.P. Toro, Optimization of scramjet inlet based on temperature and Mach number of supersonic combustion, Aerospace Science and Technology 116 (2021) 106864.
- 24. L.F. Henderson, Maximum total pressure recovery across a system of n shock waves, AIAA Journal 2 (1964) 1138–1140.
- 25. E.H. Hirschel, Basics of Aerothermodynamics: Second, Revised Edition, Springer International Publishing, Cham, 2015.
- 26. C. Park, Assessment of two-temperature kinetic model for ionizing air, J Thermophys Heat Tr 3 (1989) 233–244.
- 27. L.D. Landau, E. Teller, On the Theory of Sound Dispersion, Phys. Z. Sowjetunion 10 (1936) 147–153.
- 28. R.C. Millikan, D.R. White, Systematics of vibrational relaxation, The Journal of Chemical Physics 39 (1963) 3209–3213.
- 29. D. Li, C. Dai, B. Sun, X. Chen, Method of characteristics with thermo-chemical non-equilibrium for high Mach number inlet, Physics of Fluids 37 (2025) 026112.
- 30. V. Casseau, R.C. Palharini, T.J. Scanlon, R.E. Brown, A two-temperature open-source CFD model for hypersonic reacting flows, part one: Zero-dimensional analysis, Aerospace 3 (2016) 34.
- 31. V. Casseau, D.E.R. Espinoza, T.J. Scanlon, R.E. Brown, A two-temperature open-source CFD model for hypersonic reacting flows, part two: Multi-dimensional analysis, Aerospace 3 (2016) 34.
- 32. F. Grasso, S. Pirozzoli, Nonequilibrium Effects in Near-Wake Ionizing Flows, AIAA Journal 35 (1997) 1151–1163.